
Optimization method of Hadamard coding plate in γ -ray computational ghost imaging

Zhi Zhou ¹, Sangang Li ^{1,2*}, Qingshan Tan ¹, Li Yang ^{3,4}, Mingzhe Liu ¹, Ming
Wang ¹, Lei Wang ¹, Yi Cheng ¹

1 College of Nuclear Technology and Automation Engineering, Chengdu University of Technology, Chengdu,
610059, China

2 Applied Nuclear Technology in Geosciences Key Laboratory of Sichuan Province, Chengdu University of
Technology, Chengdu, 610059, China

3 Institute of Plasma Physics, Hefei Institutes of Physical Science, Chinese Academy of Science, Hefei 230031,
China

4 University of Science and Technology of China, Hefei 230026, China

Corresponding author:

Sangang Li

Chengdu University of Technology

Chengdu

Sichuan 610059

China

E-mail: lisangang@cdut.edu.cn

Abstract

Owing to the constraints on the fabrication of γ -ray coding plates with many pixels, few studies have been carried out on γ -ray computational ghost imaging. Thus, the development of coding plates with fewer pixels is essential to achieve γ -ray computational ghost imaging. Based on the regional similarity between Hadamard subcoding plates, this study presents an optimization method to reduce the number of pixels of Hadamard coding plates. First, a moving distance matrix was obtained to describe the regional similarity quantitatively. Second, based on the matrix, we used two ant colony optimization arrangement algorithms to maximize the reuse of pixels in the regional similarity area and obtain new compressed coding plates. With full

sampling, these two algorithms improved the pixel utilization of the coding plate, and the compression ratio values were 54.2% and 58.9%, respectively. In addition, three undersampled sequences (the Harr, Russian dolls, and cake-cutting sequences) with different sampling rates were tested and discussed. With different sampling rates, our method reduced the number of pixels of all three sequences, especially for the Russian dolls and cake-cutting sequences. Therefore, our method can reduce the number of pixels, manufacturing cost, and difficulty of the coding plate, which is beneficial for the implementation and application of γ -ray computational ghost imaging.

Key words: γ -ray computational ghost imaging; Regional similarity; Hadamard coding plate;

1. Introduction

Computational ghost imaging (CGI), which is less expensive than traditional γ -ray imaging, can reduce the scientific costs.^[1] By replacing the traditional detectors with bucket detectors and spatial modulators, CGI has attracted much attention as a new type of imaging.^[2] Moreover, the crosstalk noise between the detectors and the radiation intensity significantly affects the image quality. CGI can effectively avoid crosstalk noise between detectors and reduce the radiation intensity required by imaging. In particular, it avoids the limitation of the size of detectors on image spatial resolution, which offers a new possibility for more precise radiation imaging.

However, designing and manufacturing a suitable spatial modulator has always been a challenge for achieving CGI. The earliest breakthrough is visible light. A spatial light modulator (SLM)^[3] or digital micromirror (DMD)^[4, 5] has been used to modulate the light field. However, neither the SLM nor the DMD can modulate ray particles with certain penetration ability. In the field of rays, the only way to achieve this is to take advantage of the attenuation of rays by coding plates.

The difficulty of fabricating coding plates significantly delays the realization of X-ray and neutron ghost imaging. In 2020, He et al.^[6, 7] used electroplating to fabricate Hadamard coding plates made of Au and photochemical etching to fabricate Hadamard coding plates made of Cu. Their pixel sizes were 10×10 and $150 \times 150 \mu\text{m}$, and their thicknesses were 10 and 150 μm , respectively. Using the two coding plates as spatial

modulators, they achieved X-ray CGI with resolutions of 10 and 150 μm . In a subsequent study of neutron CGI, He et al.^[8] used the Bosch process for deep silicon etching and Gd_2O_3 powder filling to produce a thermal neutron coding plate with a thickness of 300 μm . They also conducted the first thermal neutron CGI experiment on the Dongguan spallation neutron source device.

However, few studies on γ -ray CGI are available at this moment. This is because the penetration ability of γ -rays is generally higher than that of X-rays and thermal neutrons. For example, if the energy of γ -rays is above 100 keV, the thickness required for high Z-encoding plates must be more than 1 mm, which is currently impossible to achieve using etching processes. Similar devices are also needed in γ cameras to correct γ rays, such as those in the uniformly redundant arrays coding plate (URA) and modified uniformly redundant arrays coding plate (MURA).^[9] These coding plates are made by cutting the metal into N small blocks. Each small metal block is then placed into a coding plate according to the numerical distribution of the respective correction matrices. However, to achieve the same imaging resolution, N^2 pixels are required in the CGI coding plate. It is difficult to employ this method to create coding plates with many pixels.

In addition, to achieve a higher imaging resolution, the number of required measurements has increased dramatically, and the number of subcoding plates required has also increased significantly, resulting in a very large number of pixels on the coding plate. This eliminates the cost advantage of a single-pixel imaging system, and the cost savings from detectors are wasted on coding plate manufacturing. For a high-quality γ -ray imaging system, it is difficult to create coding plates with a large number of pixels. Therefore, the development of coding plates with fewer pixels is essential to achieve γ -ray CGI.

To date, few good solutions to this problem have been reported. The reasons for this are as follows: (1) relevant research is insufficient because of the short history of ray CGI; (2) in the optical field, it is easy to change the distribution of modulated light fields because of the widespread use of SLM and DMD. The study of light-field modulation mainly focuses on achieving high-quality imaging under sampling.

If the undersampling method is used in γ -ray CGI, the number of required coding plate pixels can also be reduced. Nevertheless, this is still excessive for γ -ray CGI. It will be easier to fabricate coding plates that are suitable for γ -rays if the number of pixels is reduced further.

Compressed sensing (CS) theory provides an excellent theoretical framework for image reconstruction in CGI with undersampling. It often uses some special measured patterns, such as the Hadamard mask and random mask, and iterative optimization methods, such as the L1-magic algorithm, orthogonal matching pursuit (OMP) algorithm, and TVAL3 algorithm, for image reconstruction.^[10] The undersampling method can reduce the number of pixels required by the coding plates, but this also means a higher standard in the design of coding plates.^[11-13] That is to say, in the limited number of measurements, the coding plate should maximize the degree of "fluctuation" of the measurement data so that valid information can be retained as much as possible.^[14-16] Random masks have the advantage of being easy to manufacture. One effective method to reduce the sampling rate further is to use orthogonal basis types of masks, such as Hadamard coding plates, to remove the redundancy in random measurements.

Currently, Hadamard coding plates are widely used in CGI. Hadamard coding plates are adopted because the Hadamard matrix has some interesting features, such as good orthogonality and the ability to remove redundant information in natural scenes.^[17] Then, the question arises, which subcoding plates should be selected to form a new plate as small as possible and able to maintain high-quality imaging? Researchers have proposed various undersampling measurement sequences based on the Hadamard matrix. They hope that the careful design of multiplexing matrices will result in potential performance improvements in CGI.

Sun et al.^[16] proposed a Russian doll measurement sequence in 2017. This sequence was designed according to both the characteristics of the numerical distributions and the total number of subcoding plate blocks. This sequence can achieve good recovery results, with a sampling rate of only 16%. In 2019, Yu et al.^[18] found that rearrangement of the measurement sequence of Hadamard coding plates might

change the coherent area of each imaging point, which might in turn lead to a change in the quality of imaging. If the measurement sequence of the coding plates is arranged in ascending order in terms of the number of blocks, the coherent region of each imaging point will naturally become smaller, resulting in a high-quality imaging recovery at smaller sampling rates. This measurement sequence, known as the "cake-cutting" sequence, has a better effect than the Russian dolls and random Hadamard measurement sequences in undersampling. In addition, because the image reconstruction effect of the compressed sensing algorithm is closely related to the selected sparse matrix, some researchers have proposed measurement sequences based on different sparse matrices, such as the Harr sequence.^[19, 20] At a sampling rate of 25%, this Harr sequence can better restore the image characteristics.

In 2020, Xiao proposed two new measurement sequences from the perspective of graph decomposition: the total variation (TV) method and the total wavelet transformed coefficients (TW) method.^[21] The subcoding plates are reordered through their TV and TW in ascending order to achieve the best performance. The numerical simulation and experimental results show that the TV, CC, and TW orders can provide almost the same reconstruction at deep compressive sampling, and even better performance at a sampling ratio above 30%.

Yu proposed a concept called selection history, which can record the Hadamard spatial folding process, and built a model based on it to reveal the formation mechanisms of different orderings and deduce the mutual conversion relationship among them.^[17] Based on this, a weight ordering of the Hadamard basis was proposed. Both the numerical simulation and experimental results have shown better reconstruction quality with a lower sampling rate than traditional sorting methods.

Many orderings have emerged, but their relations remain unclear and lack a unified theory to explain the inherent math and physical mechanisms. In particular, there is a lack of mathematical explanation as to why good imaging quality can be obtained for each undersampling sequence. In addition, most researchers have concentrated on how to compose a multiplexing matrix in the undersampling method to reduce the number of pixels of the coding plates (mask). However, the method that directly reduces the

number of pixels of the coding plates by changing the connection between the subcoding plates is ignored.

In this study, on the premise that the size of coding boards cannot be reduced on a large scale owing to the unification of interpretation theories at present, the internal correlation of the subcoding plate is studied from another perspective, and the new connection mode between subcoding boards is studied to reduce the number of pixels of coding plates.

The specific approach is as follows: we propose an optimization algorithm that can create “compressed coding plates.” A compressed coding plate is generated by compressing a traditional coding plate. The algorithms satisfy the requirements of both full sampling and undersampling. This study consisted of three parts.

- 1) The characteristics of Hadamard coding plates were studied, and a moving distance matrix was obtained to quantify the regional similarity between the subcoding plates.
- 2) Two ant colony optimization arrangement algorithms were designed to reuse pixels of the same region to the largest degree between the subcoding plates.
- 3) The optimum method was tested, and its outcomes were discussed in terms of full sampling and undersampling.

2. Methods

2.1 Computational ghost imaging

The schematic of a common γ -ray CGI device is shown in Fig. 1.

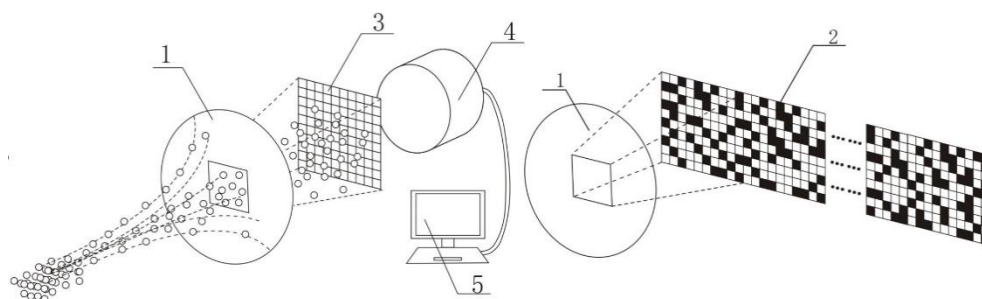


Fig. 1 Conceptual drawing of the experimental setup used for γ -ray CGI. The left and right parts of the image show the overall layout and a partial enlargement of the equipment, respectively. The collimator (1) ensures that the particles produced by the γ -source are only

incident on the imaging area; the coding plate (mask) (2) is composed of all the subcoding plates, whose pattern is encoded on metal; the particles are modulated on the subcoding plate (3), and the object can be placed between the collimator and subcoding plate; the signal-pixel detector (4) collects the intensity of rays; a computer (5) is used to reconstruct the images.

In CGI, it is necessary to move the coding plate after each measurement to change the shape of the mask in the imaging area and thus, the distribution of the ray field. In this study, the mask of the corresponding part of each measurement is called a subcoding plate. The measurement process can be expressed using Eq. 1:

$$I_i = P_i * O \quad (1)$$

where

O represents $N \times N$ pixel values in an object and is transformed into a column vector.

P_i represents $N \times N$ modulation values corresponding to the i th subcoding plate (a measured pattern) and is transformed into a row vector.

I_i represents a measured value obtained from the i th measurement.

In CGI, the measured value I_i is mathematically equivalent to the inner product of each pattern P_i and object image O . The spatial information of objects is acquired by a detector and subcoding plates, not by array detectors.

Traditional ghost imaging is a well-known imaging technique. Its definitions are as follows. An object image O_r can be reconstructed using P_i and I_i .

$$O_r * (x, y) \approx \langle I_i P_i(x, y) \rangle - \langle I_i \rangle \langle P_i(x, y) \rangle \quad (2)$$

where $\langle . \rangle$ denotes the average of all the CGI measurements.

With the development of ghost imaging technology, some researchers have reconstructed images from the perspective of solving equations. For example, Zhang proposed pseudo-inverse ghost imaging^[21] and Xue proposed singular value decomposition ghost imaging.^[22] Then, optimization algorithms based on compressed sensing (CS) have been employed to reconstruct images under undersampling, such as

the orthogonal matching pursuit (OMP) and TVAL3 algorithms.

In addition, some patterns, such as the Gaussian, Bernoulli, DCT, and Hadamard matrices, have been used in CGI. The Hadamard matrix can generate better-quality images compared to other measurement matrices.^[17] Therefore, the Hadamard coding plate is widely used in CGI.

2.2 Regional similarity

Because of the uncorrelated character of any two columns or rows, the Hadamard matrix, as a modulation orthogonal matrix, can effectively avoid correlation noise among the pixels, and the reconstructed image quality can be greatly improved at the same sampling rate.^[14] The Hadamard matrix is generally constructed recursively from low to high order, as shown below:

$$H_{2^n} = \begin{bmatrix} H_{2^{(n-1)}} & H_{2^{(n-1)}} \\ H_{2^{(n-1)}} & -H_{2^{(n-1)}} \end{bmatrix} \quad (3)$$

The traditional Hadamard coding plate comprises $K \times K$ -block subcoding plates. The molding method of the subcoding plates converts the 1D code elements into 2D patterns, as shown in Fig. 2(a–c).

Owing to the recursive property of the Hadamard matrix, it can be observed that the front part of a row in the matrix is the same as the back part of another row (Fig. 2(a)). This rule causes the left area (Fig. 2(b)) of one subcoding plate to be completely consistent (Fig. 2(d)) with the right area (Fig. 2(c)) of another subcoding plate. This phenomenon is known as regional similarity between two subcoding plates.

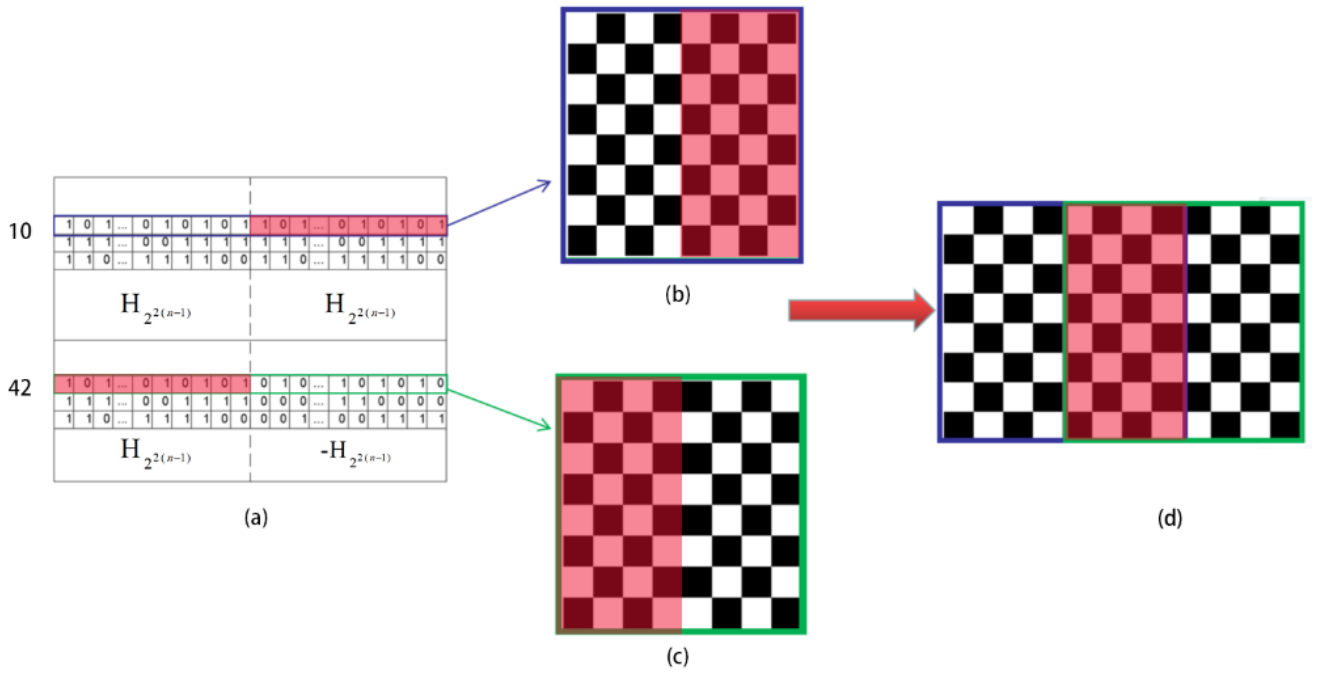


Fig. 2 Modeling method of subcoding plates and regional similarity between subcoding plates. (a) Partial numerical distributions of the Hadamard matrix with a size of 64^2 order; (b) and (c) represent two subcoding plates forming the 10th and 42nd rows of the matrix, respectively, which are clearly marked by purple and green borders, and the regions of same pixel values are marked in red; the two subcoding plates were compressed according to the regional similarity (d).

Table 1 Moving distance matrix between all subcoding plates

No.	C1	C2	C3	C4	C5	C6	C7	C8	C9	C10	C11	C12	C13	C14	C15	C16	C17	C18	C19	C20	C21	C22	C23	C24	C25	C26	C27	C28	C29	C30	C31	C32	C33	C34	C35	C36	C37	C38	C39	C40	C41	C42	C43	C44	C45	C46	C47	C48	C49	C50	C51	C52	C53	C54	C55	C56	C57	C58	C59	C60	C61	C62	C63	C64																																																																																																																																																																																																																																																																																																																																																																																																																																																																																																																																																																																																																																																																																																																																																																																																																																																																																																																																																																																																																																																																																																																																																																																																																																																														
C1	inf																																																																																																																																																																																																																																																																																																																																																																																																																																																																																																																																																																																																																																																																																																																																																																																																																																																																																																																																																																																																																																																																																																																																																																																																																																																																																																																													

subcoding plate C_i . The value of regional similarity represents the number of columns in the same part between the left area of C_m and the right area of C_n .

If we want to use regional similarity to compress the coding plate, it is necessary to calculate the degree of regional similarity between subcoding plates quantitatively. To achieve this goal, a moving distance matrix M is employed to describe the regional similarity. The moving distance matrix M_{64} corresponding to the Hadamard matrix with a size of 64^2 (64 subcoding plates) is presented in Table 1.

According to the matrix in Table 1, the regional similarity between the subcoding plates has the following characteristics.

- 1) Approximately 90% of the elements in the moving distance matrix take the value of 8, which indicates that there is no regional similarity between most subcoding plates. However, there are 320 pairs of subcoding plates with regional similarities, which indicates that the aim of reducing the number of pixels of the coding plates can be achieved by adjusting the order of the subcoding plates.
- 2) In the matrix, there is a sporadic continuous oblique distribution of low-value elements, which indicates that there are interrelated characteristics between subcoding plates with regional similarities. This makes it possible to use continuous subcoding plates with regional similarities.

Therefore, based on the moving distance matrix, we reuse the same region between the subcoding plates to reconstruct a new coding plate with fewer pixels, as shown in Fig. 2(d). The new coding plate can compress a traditional coding plate and is called a compressed coding plate.

2.3 Ant colony optimization arrangement algorithms

2.3.1 Ant colony algorithms

To maximize the use of regional similarity between the subcoding plates and thus minimize the pixels of the compressed coding plate, it was necessary to redesign a measurement sequence of the subcoding plates according to the moving distance matrix obtained in the previous section. The problem is modeled as follows.

$$\begin{aligned}
& \text{Min} \quad S = \sum_{t=1}^{N-1} m(i_t, j_t) \\
& \quad j_t = i_{t+1} \\
& \quad i_{t+1} = i_t \\
& \text{s.t.} \quad i \in [1, 2, 3, \dots, N] \\
& \quad i_t \neq i_j \text{ and } \{j \mid j \in [1, 2, \dots, i_t] \cap (i_t, i_t + 1, \dots, N]\}
\end{aligned} \tag{4}$$

where N represents the number of points in a set; m_{ij} represents the distance from point i to point j , and the distance between points can be expressed by moving matrix M ; S represents the sum of all distances in a path; t represents the t th point in a path, and it ensures that the distance between adjacent points is calculated.

In the model, the goal is to find a path that minimizes S ; the constraints are as follows: 1) each point can only pass once; and 2) all points need to be passed. This problem is similar to the travelling salesman problem (TSP). It is a mathematical combinatorial optimization problem and an N-P problem. The ant colony algorithm is a mature and effective algorithm for solving the TSP and other combinatorial optimization problems.^[23] In this study, each subcoding plate was used as the node of the ant colony path space, and the moving distance matrix was used as the node spacing. The path of an ant passing through all nodes is a feasible solution to the problem, and all the paths of the entire ant population constitute a feasible solution space.

Affected by the communication mechanism of ants, their release of pheromones, and the volatilization mechanism of pheromones, more pheromones will be released on the short path (the optimal solution), whereas the pheromones on other solutions will volatilize slowly with iterations. Ants prefer paths with high pheromone concentrations. As the number of iterations increases, more pheromones remain on a shorter path and more ants choose this path. Eventually, under the action of positive feedback, ants choose the best path, and the corresponding subcoding plate sequence is the optimal solution to this problem.

In addition, when ant k is at point t , the probability ($P_{ij}^k(t)$) of choosing the next point j from point i mainly considers two factors: first, the distance between points i and j , which is called the heuristic factor $\eta_{ij}(t)$. Second, the feasibility from points i

and j , which is called pheromone concentration $\tau_{ij}(t)$. $P_{ij}^k(t)$ can be calculated using the following formula:

$$P_{ij}^k(t) = \begin{cases} \frac{[\tau_{ij}(t)]^\alpha [\eta_{ij}(t)]^\beta}{\sum_{j \in j_k} [\tau_{ij}(t)]^\alpha [\eta_{ij}(t)]^\beta}, & j \in j_k \\ 0, & j \notin j_k \\ \eta_{ij} = \frac{1}{m_{ij}} \end{cases} \quad (5)$$

where α represents the importance of pheromones, β represents the importance of the heuristic factor, and $j_k(t)$ is a selectable point set.

After obtaining the path of the generation ant, the path is used to update the pheromones. The updated formula is as follows:

$$\begin{aligned} \tau_{ij}(t+1) &= (1-\rho)\tau_{ij}(t) + \Delta\tau_{ij} \\ \Delta\tau_{ij} &= \sum_{n=1}^{N_{ant}} \Delta\tau_{ij}^n \\ \Delta\tau_{ij}^n &= \frac{Q_{ant}}{L_n} \end{aligned} \quad (6)$$

where ρ is the volatilization coefficient of pheromones, N_{ant} is the number of generation ants, $\Delta\tau_{ij}$ is the sum of pheromones left by ants on the path between point i and point j , $\Delta\tau_{ij}^k$ is the pheromone left by the k th ant on the path between point i and point j , Q_{ant} is the total pheromone of an ant, and L_k is the total length of the path taken by the k th ant.

2.3.2 Method for optimum coding plate

According to the algorithm described in Section 2.3.1, the measurement sequence of the subcoding plates under the maximum use of regional similarity can be calculated. However, the coding plate manufactured according to the sequence is very long. Considering the actual production and usage, we need to optimize the coding plate further. A compressed coding plate should be designed, which should have a rectangular shape. Thus, it is called a rectangular compressed coding plate. This means that there

should be no significant difference in terms of the length of each segment of the coding plate, and the total number of pixels of the compressed coding plate should be minimized. To solve the above problems, two methods can be employed for obtaining the optimum coding plate: the one-objective ant colony segmentation algorithm (OACSA) and the multi-objective ant colony reconstruction optimization algorithm (MACRA).

(1) One-objective ant colony segmentation algorithm

The core idea of this method is that the long measurement sequence obtained by the ant colony algorithm is divided into multiple short measurement sequences by selecting the appropriate segmentation points, and the long measurement sequence does not need to be changed. These short measurement sequences are reconstructed to obtain the corresponding rectangular compressed coding plates (supplemental pixels and parallel combinations). The reconstruction process may cause an increase in the total number of pixels in the coding plate. After the analysis, the position of the segmentation point should meet the following three criteria:

- 1) The length of each segment is approximately equal.
- 2) The segmentation points should be carefully selected to preserve the completed subcoding plate to avoid unnecessary pixel supplementation.
- 3) The segmentation points should be selected between the subcoding plates with low regional similarity to ensure that the number of supplemental pixels involved in the reconstruction process is small.

Based on these three criteria, this study proposes a segmentation-point selection method for a single-sequence coding plate, and its flowchart is shown in Fig. 3. According to the segmentation point selected by the algorithm, the single-sequence coding plate is divided to obtain multiple coding plate segments. Then, multiple segments are reconstructed to obtain the corresponding compressed coding plate (supplemental pixels and parallel combination).

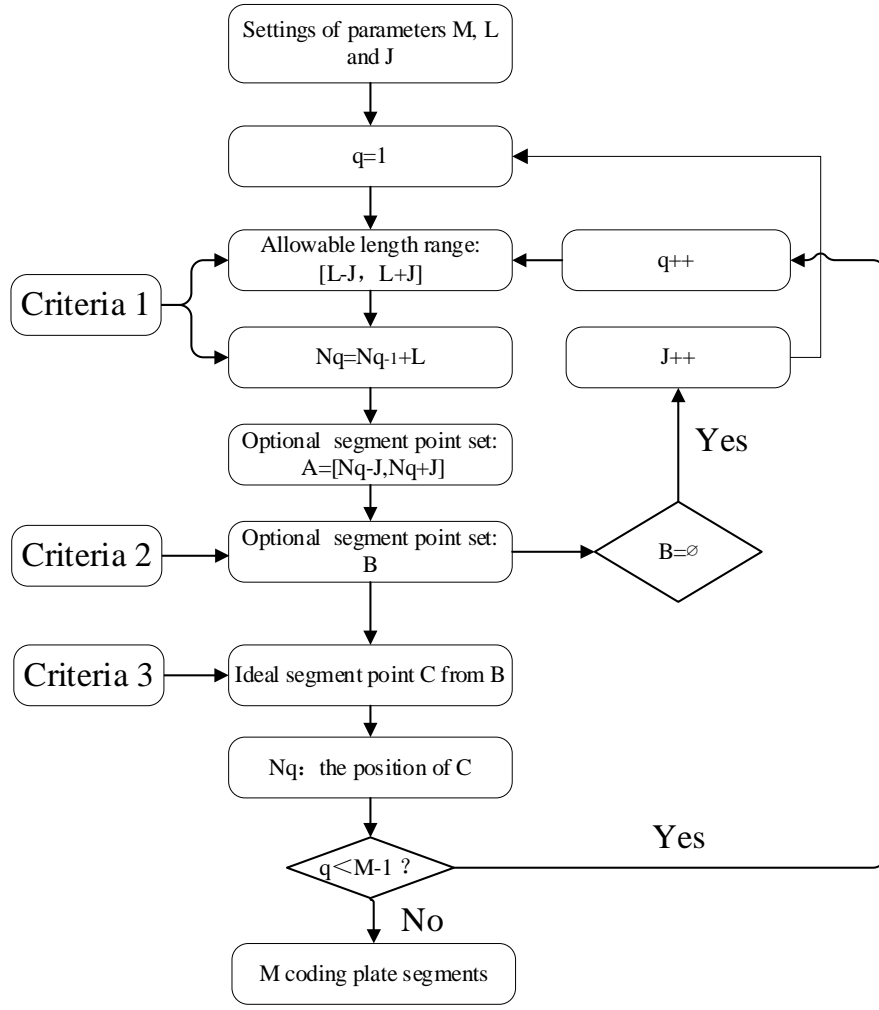


Fig. 3 Segmentation-point selection method for a single-sequence coding plate

Note: M represents the number of segments, L represents the mean length of each segment, J represents the allowable length deviation in each segment, N_q represents the location of the q^{th} ideal segmentation point, and $N_0 = 0$; M represents the number of segments and $M = \text{floor}(\sqrt{\frac{L_{\text{All}}}{K}})$;

L_{All} represents the length of a single-sequence compressed coding plate; K is the order of the subcoding plate.

(2) Multi-objective ant colony reconstruction optimization algorithm

The reconstruction of a rectangular compressed coding plate is a problem of reconstructing multiple independent segments and is an optimization problem with constraints. To solve this problem, we included the constraint (each segment is essentially of the same length) as the penalty part in the objective function, as shown in Eq. 7.

$$\begin{aligned} \text{Min} \quad S &= \sum_{k=1}^{N_{seg}} s_k + \gamma * \max(s_1, s_2, s_3, \dots, s_{N_{seg}}) \\ \text{where:} \quad s_k &= \sum_{i=1}^{N_k} m(i, j_i) \end{aligned} \quad (7)$$

where N_{seg} is the total number of segments and also represents the number of ants. s_k is the distance traveled by the k th ant in the same group, and it represents the length of the k th segment, N_k represents the number of points that the ant needs to cross, and γ is the penalty factor coefficient.

The MACRA was employed to solve the model. Through continuous iterative optimization, the total distance was gradually reduced, and the gaps between the lengths of all segments were bridged in the multi-objective colony algorithm.

2.4 Evaluation index

For a quantitative measurement of the degree of reduction in the number of pixels of the coding plate with ant colony optimization arrangement algorithms, this study defined a quantitative index-compression ratio, α . It represents the ratio of the number of pixels between the compressed and traditional coding plates. The smaller the value, the better the compression effect. Its formulas are as follows:

$$\begin{aligned} \alpha &= \frac{\sum_{i=1:M} D_i}{K^4} \\ D_i &= \left(\sum_{j=1:P_i-1} d_{i,j} + K \right) \times K \end{aligned} \quad (8)$$

where D_i represents the number of pixels for the i th segment, K represents the order of a subcoding plate, P_i represents the number of subcoding plates in each segment, $d_{i,j}$ denotes the minimum movement distance from the j th to the $(j+1)$ th subcoding plate in the i th segment, the value of i varies from 1 to M , and M is the number of segments.

3. Results and discussions

We applied the ant colony optimization arrangement algorithms described in Section 2 to reconstruct the full sampling traditional Hadamard coding plate and obtain a compressed coding plate.

Subsequently, to demonstrate the feasibility of undersampling, we obtained the

compression ratios of compressed coding plates corresponding to the Harr, cake-cutting, and Russian dolls sequences at different sampling rates. The compression effects were compared and analyzed.

3.1 Compressed coding plate in full sampling

For all the subcoding plates corresponding to the 1024-order Hadamard matrix, the regional similarity between the subcoding plates was quantified using the moving distance modeling method to obtain the moving distance matrix. The OACSA and MACRA (the main parameters of the two algorithms are listed in Table 2) were used to reconstruct the rectangular Hadamard compressed coding plates, which are shown in Fig. 4. The compression results are shown in Fig. 5.

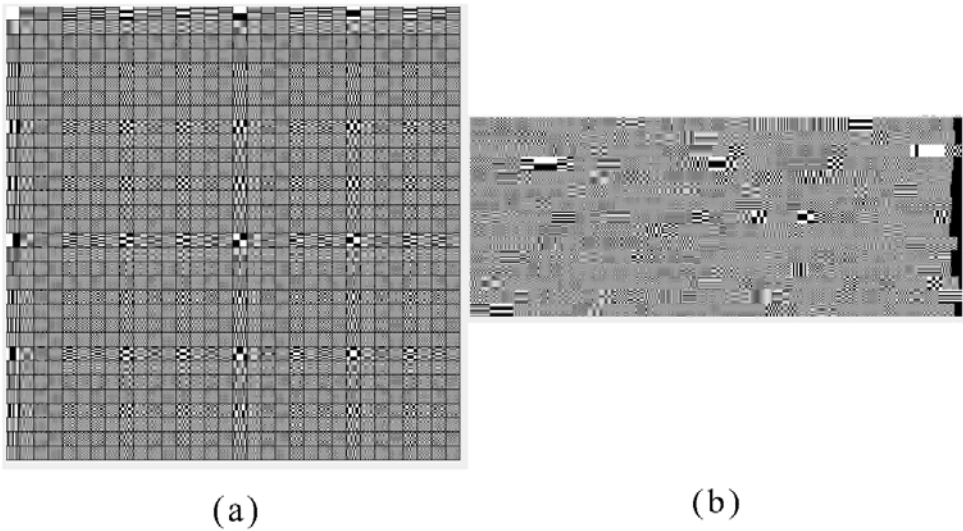


Fig. 4 Traditional and rectangular compressed coding plate.

(a) Traditional coding plate in full sampling, (b) compressed coding plate in full sampling.

Table 2 Main parameters of the ant colony optimization arrangement algorithms

Parameter name	Colony size	Iteration number	Importance of pheromones	Pheromone evaporation rate	Heuristic factor coefficients	Segment number
Value	10240	10240	1	0.5	1	16

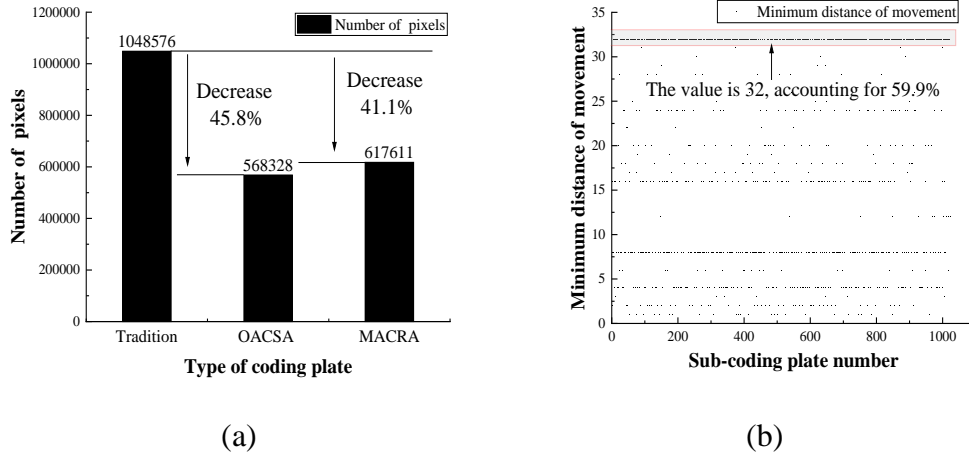


Fig. 5 Experimental results in full sampling. (a) Compression results of the ant colony optimization algorithms in full sampling; (b) minimum movement distance between adjacent subcoding plates in the single-sequence coding plate.

As shown in Fig. 5(a), both the OACSA and MACRA can significantly reduce the number of pixels, and their corresponding compression rates α are 54.2% and 58.9%, respectively. Moreover, the OACSA has a better compression effect. The reasons for this are as follows:

With constraints, the MACRA is the basic solution to this optimization problem of combination, but it is more complicated than the OACSA. The MACRA requires a long time to obtain an answer. The answers are easily affected by the original figures. We believe that the OACSA may be a better solution to this challenging problem. The OACSA was applied in two phases:

Phase 1: Without constraints (to make the coding plates rectangular), the one-way ant colony algorithm in the OACSA can solve the optimization problem. It is relatively simple and single-sequence coding plates with very few pixels can be made.

Phase 2: When constraints are involved, single-sequence coding plates are segmented and combined to create rectangular compressed coding plates. If appropriate segmentation points are selected through the segmentation point selection method, the entire process results in only a minor increase in the number of pixels.

The minimum distances of movement between adjacent subcoding plates in the

single-sequence coding plate generated from the OACSA are shown in Fig. 5(b). It can be observed that the points with a maximum value of 32 and minimum moving distance account for 59.9%, and their distribution is wide. This phenomenon is favorable for the segmentation point selection method; thus, only a small number of pixels are added. This means that there is no significant difference between the number of pixels in the rectangular compressed coding plate and the single-segment arrangement scheme. Thus, we conclude that the OACSA is better than the MACRA.

3.2 Compressed coding plate in undersampling

In the previous section, it was proven that both optimum algorithms have good compression effects for the Hadamard coding plate in full sampling; however, the undersampling compression effects of the algorithm are unknown. Therefore, in this section, for the Harr, Russian dolls, and cake-cutting sequences, the OACSA, which has a better compression effect, is applied to reconstruct compressed coding plates at sampling rates of 5%–40%. The α values of the compressed coding plates are shown in Figure 6(a).

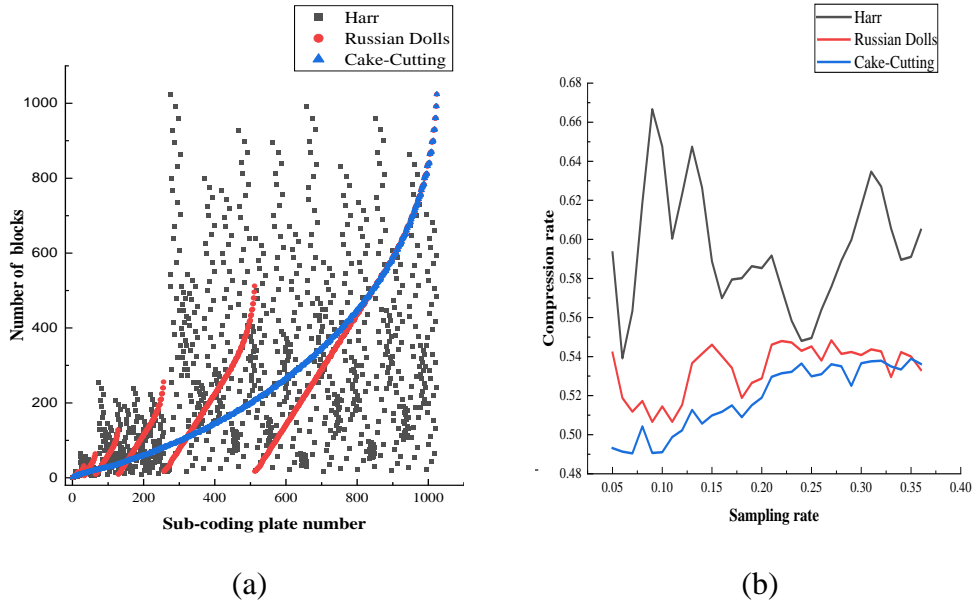


Fig. 6 Experimental results in undersampling. (a) Compression ratio of three sequences at different sampling rates; (b) trends of the number of blocks of the sub-coding plates in different sequences.

As shown in Fig. 6(a), the ant colony optimization arrangement algorithm has a certain compression effect on the three sequences at different sampling rates, especially the Russian dolls and cake-cutting sequences. The reduction in the number of pixels in the two sequences can reach 40%.

According to relevant literature^[16, 18], the Russian dolls sequence can achieve a good imaging result at a sampling rate of 25%, that is, the number of pixels required for the coding plate is 25% of the number of pixels of the traditional Hadamard encoding plate. If the coding plate is compressed using the optimization arrangement algorithm, the number of pixels can be further reduced and the same imaging effect can be achieved without changing the modulation matrix. Therefore, the use of both the undersampling method and the ant colony optimization arrangement algorithm will significantly reduce the number of pixels in the coding plate. This will help lower the difficulty and cost of manufacturing the encoding plate and consequently build the foundation for the realization of γ -ray CGI.

In addition, the compression effect of the cake cutting sequence is the greatest, followed by the effect of the Russian dolls sequence, whereas that of the Harr sequence is not obvious. This result shows that the ant colony optimization arrangement algorithm has different compression effects on different types of sequences. The main reasons for this are as follows:

A large area of the same pixel values is likely to appear between the subcoding plates with a small or similar number of blocks, that is, regional similarities can be easily found between such subcoding plates.

The cake-cutting sequence is arranged in ascending order of the number of blocks. Russian dolls sequences are designed to take advantage of the fact that higher-order Hadamard matrices ($H_{2^{2n}}$) contain low-order Hadamard matrices ($H_{2^{2m}}$, $m < n$). In their specific sorting method, patterns of subcoding plates with scaled versions of low-order matrices will be preferentially measured. Then, subcoding plates with a low number of blocks will also be preferentially measured. This method results in the cyclic growing trend of the number of blocks of Russian dolls. The Harr sequence is arranged

in ascending order of the Harr value of the subcoding plate. According to these three different sorting rules, the trends of the number of blocks of the subcoding plates of different sequences are shown in Fig. 6(b). Both the cake-cutting and Russian dolls sequences are sorted in connection with the number of blocks, whereas the Harr sequence is not. As a result, the compression effects of the cake-cutting and Russian dolls sequences are much better than that of the Harr sequence.

4. Conclusion

In this study, optimum ant colony algorithms based on regional similarity are proposed to reduce the number of pixels and reconstruct a rectangular compressed coding plate. Without sacrificing the imaging quality, their compression rates can reach 60% in full sampling. In undersampling, the proposed algorithm has a certain compression effect on each of the three sequences at different sampling rates, and the effects are obvious on the Russian dolls and cake-cutting sequences. The use of both undersampling and the proposed algorithm significantly reduces the number of pixels in the coding plate. This will help reduce the difficulty and cost of manufacturing the encoding plate and build the foundation for the realization of γ -ray CGI. Finally, in addition to γ -ray CGI, the proposed algorithms can also be applied to other types of CGI that require modulation by mechanical movement of the coding plate.

Acknowledgments

The authors would like to acknowledge the support of The Youth Science Foundation of Sichuan Province with grant No. 22NSFSC3816 and No. 2022NSFSC1231, the General Project of the National Natural Science Foundation of China with grant No. 12075039 and No. 41874121, and the Key Project of the National Natural Science Foundation of China with grant No. U19A2086.

Author contributions

All authors contributed to the study conception and design. Material preparation, data collection and analysis were performed by Zhi Zhou, Sangang Li, Qingshan Tan. The first draft of the manuscript was written by Zhi Zhou, and all authors commented on previous versions of the manuscript. All authors read and approved the final

manuscript.

Reference

1. Y. Bromberg, O. Katz, Y. Silberberg., Ghost imaging with a single detector. *Physical Review A*. 79, 053840 (2009). doi:10.1103/PHYSREVA.79.053840
2. G.M. Gibson, S.D. Johnson, M.J. Padgett. Single-pixel imaging 12 years on: a review. *Optics express*, 28, 28190-28208 (2020). doi:10.1364/OE.403195
3. J.H. Shapiro., Computational ghost imaging. *Physical Review A*, 78, 6 (2008). doi:10.1364/IQEC.2009.IThK7
4. D. Takhar, J.N. Laska, M.B. Wakin et al., A new compressive imaging camera architecture using optical-domain compression. *SPIE* 6065, 43 (2006). doi:10.1117/12.659602
5. M. Chen, E. Li, S. Han., Application of multi-correlation-scale measurement matrices in ghost imaging via sparsity constraints. *Applied optics*, 53, 13 (2014). doi:10.1364/AO.53.002924
6. Y.H. He, A.X. Zhang, W.K. Yu et al., Energy-selective x-ray ghost imaging. *Chinese Physics Letters*, 37, 4 (2020). doi:10.1088/0256-307X/37/4/044208
7. Y.H. He, A.X. Zhang, M.F. Li et al., High-resolution sub-sampling incoherent x-ray imaging with a single-pixel detector. *APL Photonics*, 5, 5(2020). doi:10.1063/1.5140322
8. Y.H. He, Y.Y. Huang, Z.R. Zeng et al., Single-pixel imaging with neutrons. *Science Bulletin*, 66, 2 (2021). doi: 10.1364/CLEOPR.2020.C1G_1
9. T. Zhang, L. Wang, J. Ning et al., Simulation of an imaging system for internal contamination of lungs using MPA-MURA coded-aperture collimator. *Nucl. Sci. Tech*, 32, 2 (2021). doi:10.1007/S41365-021-00849-3
10. Y. Ren, P. He, H.L. Wang., Compressed sensing and Otsu's method based binary CT image reconstruction technique in non-destructive detection. *Nucl. Sci. Tech*, 26, 5 (2015). doi:10.13538/j.1001-8042/nst.26.050403
11. M.F. Duarte, M.A. Davenport, D. Takhar et al, Single-pixel imaging via compressive sampling. *IEEE signal processing magazine*, 25, 2 (2008). doi:10.1109/MSP.2007.914730

-
12. S.J. Olivas, Y. Rachlin, L. Gu et al., Characterization of a compressive imaging system using laboratory and natural light scenes. *Applied optics*, 52, 19 (2013). doi: 10.1364/AO.52.004515
 13. P.G. Vaz, D. Amaral, L.R. Ferreira et al., Image quality of compressive single-pixel imaging using different Hadamard orderings. *Optics express*, 28, 8 (2020). doi: 10.1364/OE.387612
 14. W.K. Pratt, J. Kane, H.C. Andrews., Hadamard transform image coding. *Proceedings of the IEEE*, 57, 1 (1969). dio:10.1109/PROC.1969.6869
 15. N. Radwell, K.J. Mitchell, G.M. Gibson et al., Single-pixel infrared and visible microscope. *Optica*, 1, 1 (2014). dio:10.1364/OPTICA.1.000285
 16. M.J. Sun, L.T. Meng, M.P. Edgar et al., A Russian Dolls ordering of the Hadamard basis for compressive single-pixel imaging. *Scientific reports*, 7, 1 (2017). doi: 10.1038/S41598-017-03725-6
 17. W.K. Yu, C. Cao, Y. Yang et al., Single-pixel imaging based on weight sort of the Hadamard basis. *arXiv preprint arXiv:2203.04659*.
 18. W.K. Yu, Super sub-Nyquist single-pixel imaging by means of Cake-Cutting Hadamard basis sort. *Sensors*, 19, 19 (2019). dio:10.3390/s19194122
 19. M.F. Li, X.F. Mo, L.J. Zhao et al., Single-pixel remote imaging based on Walsh-Hadamard transform, *Acta Physica Sinica*, 2665, 6 (2016). doi:10.7498/aps.65.064201
 20. M.F. Li, L. Yan, R. Yang., Fast single-pixel imaging based on optimized reordering Hadamard basis, *Acta Phys. Sin.*, 68, 6 (2019). dio: 10.7498/aps.68.20181886
 21. C. Zhang, S. Guo, J. Cao et al. Object reconstitution using pseudo-inverse for ghost imaging[J]. *Optics Express*, 22, 24 (2014). doi:10.1364/OE.22.030063
 22. Z. Xue, X. Meng, X. Yang et al. Singular value decomposition ghost imaging[J]. *Optics Express*, 26, 10 (2018). doi:10.1364/oe.26.012948
 23. M. Dorigo, G.D. Caro, L.M. Gambardella., Ant Algorithms for Discrete Optimization, *Artificial Life*, 5, 2 (1999) dio:10.1162/106454699568728